Journal of Power Sources 196 (2011) 3705–3712

Contents lists available at ScienceDirect

Journal of Power Sources

journal homepage: www.elsevier.com/locate/jpowsour

Thermal stability, oxygen non-stoichiometry, electrical conductivity and diffusion characteristics of $PrNi_{0.4}Fe_{0.6}O_{3-\delta}$, a potential cathode material for IT-SOFCs

Jeanette Rebello[a,*], Vladimir Vashook[a,b], Dimitro Trots[c], Ulrich Guth[a,b]

[a] Department of Chemistry and Food Chemistry, Dresden University of Technology, D-01062 Dresden, Germany
[b] Kurt-Schwabe Research Institute, D-04720 Ziegra-Knobelsdorf, Germany
[c] HASYLAB, Deutsches Elektronen-Synchrotron, 22607 Hamburg, Germany

ARTICLE INFO

Article history:
Received 6 September 2010
Received in revised form
14 December 2010
Accepted 3 January 2011
Available online 12 January 2011

Keywords:
IT-SOFC
Cathode material
Double-B-site mixed perovskite
Electrical conductivity
Oxygen non-stoichiometry
Chemical diffusion
Oxygen exchange

ABSTRACT

The potential use of a double B mixed-perovskite as a promising cathode material in intermediate temperature solid oxide fuel cells (IT-SOFCs) has been anticipated as a result of this work. A thorough investigation of some important parameters like thermal stability, thermal expansion, oxygen non-stoichiometry, electrical conductivity and diffusion characteristics of the $PrNi_{0.6}Fe_{0.4}O_{3-\delta}$ ceramic sample have been investigated as functions of temperature (20–1000 °C) and oxygen partial pressure (0.6–21,000 Pa). According to the measurements, the composition was phase stable at $pO_2 > 1$ Pa up to 1000 °C and shows p-type semiconductivity with a low conductivity versus pO_2 dependence.

The perovskite has been found to have comparable thermal expansion coefficients with those of commonly used solid electrolytes like CeO_2 and ZrO_2 based oxides. In case of the chemical diffusion experiments higher oxygen diffusion mobility observed during reduction processes in comparison with those during oxidation have been explained by the already known formation of neutral defect clusters.

1. Introduction

New cathode materials for use in solid oxide fuel cells (SOFCs) are constantly being studied all over the world. Out of the SOFCs that exist, intermediate temperature solid oxide fuel cells (IT-SOFCs) are very popular since they allow the use of low-cost interconnects and have less frequent problems with sealing and thermal degradation, just to name a few. Despite the advantages, one major problem faced by this type of SOFC is the fact that polarisation resistance on the cathode side is generally higher than that on the anode side leading to breakdown in the functioning of the fuel cell. Lanthanum strontium manganate (LSM) cathodes have since long been the most commonly and widely studied materials and only recently Fe–Co based perovskite cathodes have entered the scenario. Fe–Co based perovskites have many important properties out of which one is a reasonably low polarisation resistance as in the case of $La_{0.6}Sr_{0.4}Fe_{0.8}Co_{0.2}O_{3-\delta}$/Gd doped CeO_2 cathode at 600 °C [1]. Although the latter could have been a good candidate as a cathode material in IT-SOFCs, its major drawback lies in its relatively high difference in thermal expansion coefficient (TEC) as compared to that of the common electrolytes, e.g. with YSZ (difference of $7.5 \times 10^{-6}\,K^{-1}$) and with CeO_2 based oxides (difference of $(6–15) \times 10^{-6}\,K^{-1}$). Such a difference in TECs between the cathode and electrolyte would cause thermal stress at the interface during the operation of the fuel cell at high temperatures leading to cracking and delamination.

Similarly, other candidates like Fe–Ni perovskites with high electronic conductivity and comparable thermal expansion coefficients with that of CeO_2 and ZrO_2 based oxides have also been studied. Hashimoto et al. [2] have studied conductivity profiles of $PrNi_{1-x}Fe_xO_3$ ($x = 0.4–0.6$) materials at high temperature and also their impedance and polarisation curves on $Ce_{0.9}Gd_{0.1}O_{2-\delta}$(CGO10) electrolyte and compared them with $LaFe_{0.4}Ni_{0.6}O_{3-\delta}$. On the other hand, according to magnetic and electronic structure studies on similar substances carried out by Kumar et al. [3], the substitution of Ni for Fe site in $PrFeO_3$ is said to increase their conductivity and stabilise the ferromagnetic ordering.

$PrNi_{1-x}Fe_xO_3$ ceramics have been shown to have high electronic conductivity, thermal expansion coefficients comparable to CGO and hence are very promising as SOFC electrodes and oxygen per-

* Corresponding author at: Department of Inorganic Chemistry and Analytical Chemistry, University of Muenster, Correnstraße 28-30, 48149 Muenster, Germany. Tel.: +49 0251 83 33113; fax: +49 0251 83 33193.
E-mail address: j.rebello@uni-muenster.de (J. Rebello).

0378-7753/$ – see front matter © 2011 Elsevier B.V. All rights reserved.
doi:10.1016/j.jpowsour.2011.01.003

meable membranes [1]. It has to be noted, that an effective pO_2 gradient within the SOFC cathode is formed once current begins flowing. Therefore, it is particularly important to know the properties of these materials as a function of oxygen partial pressure and temperature [4,5]. Also, no data about thermal stability, oxygen non-stoichiometry, and electrical conductivity at low oxygen partial pressures (pO_2) for these compounds are available up to date. In the present investigation, we aim to study these parameters in $PrNi_{0.4}Fe_{0.6}O_{3-\delta}$ a double B mixed perovskite, as functions of temperature and oxygen partial pressure.

2. Experimental

2.1. Powder synthesis and physical characterisation

$PrNi_{0.4}Fe_{0.6}O_{3-\delta}$ powder was prepared by the solid-state reaction method. The constituent metal oxide powders Pr_6O_{11} (99% pure, Alfa Aesar), NiO (99% pure, Alfa Aesar) and Fe_2O_3 (Analytical Reagent, Reanal Hungary) were first ball-milled in an agate mill in stoichiometric amounts along with some minimum amount of ethanol for 24 h. The resultant paste was left to dry and form a mass which was ground in a mortar using a pestle to form uniform powder and then pre-calcined in air up to a temperature of 1000 °C for 17 h with a heating and cooling rate of 5 °C min^{-1}. The cooled mass was then ground again to a fine powder and then further treated as required for various experiments as discussed below. This powder pre-calcined at 1000 °C has been analysed at room temperature (RT) by XRD measurements (Siemens D5000 diffractometer, Cu K_α radiation) using a PVC sample holder.

In situ high-temperature structural studies in the temperature range from RT to 900 °C were performed at the synchrotron facility HASYLAB/DESY (Hamburg, Germany) with the powder diffractometer at beam-line B2 [6]. For this set of experiments, 0.3 mm diameter quartz capillaries were filled with powdered samples and subsequently mounted inside a STOE furnace equipped with a Eurotherm temperature controller and a capillary spinner (Debye–Scherrer geometry). The furnace temperature was measured by a Ni/CrNi thermocouple. The wavelength of 0.651254 Å was selected using a Si(1 1 1) double flat-crystal monochromator and determined from eight reflection positions of LaB_6 reference material (NIST SRM 660a). All diffraction patterns have been collected at fixed temperatures during the heating–cooling cycle using an image-plate detector [7] (2θ range 8–62°, step size of 0.004°). Additional check-patterns were taken after the heat treatment at room temperature. Data evaluation was performed using the package 'FullProf' [8], the averaged structure was analysed by the full-profile Rietveld method.

Thermal expansion coefficients were measured on porous samples in air in a LINSEIS dilatometer, temperature range of 20–850 °C with a ramp-rate of 10 °C min^{-1}. SEM images were recorded using a Zeiss DMS 982 Gemini field emission scanning electron microscope equipped with a Noran Voyager energy-dispersive spectroscopy system.

2.2. Sample preparation

Porous ceramic samples for conductivity and oxygen exchange measurements were prepared by sintering pressed bars (dimensions: 10 mm × 3 mm × 1.5 mm) in air at 1200 °C for 17 h, whereas gas dense ones for oxygen diffusion measurements were prepared by sintering similar bars at 1500 °C in air for 17 h (Fig. 1a). To check gas-tightness of the sintered samples, discs of 15 mm diameter were sintered at 1500 °C in air for 17 h. Apparatus shown in Fig. 1b was used for the examination of the discs. If the sample was porous, lower pressure was created inside the jar 4 pre-filled with helium, due to the faster diffusion of the smaller He atoms outside in comparison with the diffusion of larger N_2 and O_2 molecules from air into the jar.

2.3. Oxygen content and electrical conductivity measurements

Oxygen non-stoichiometry and electrical conductivity of the ceramic samples were investigated using a solid electrolyte measuring technique ZiroxySystem (Zirox, Greifswald, Germany)

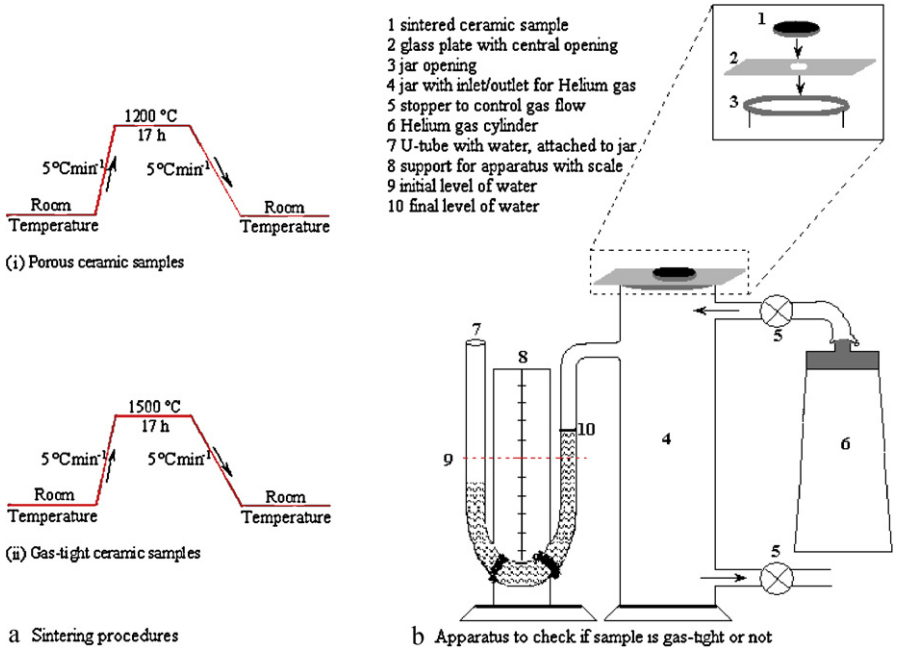

Fig. 1. (a) Schematic representations showing sintering procedures for (i) porous ceramic samples and (ii) gas-tight ceramic samples. (b) Apparatus to check if sintered sample is gas-tight or not.

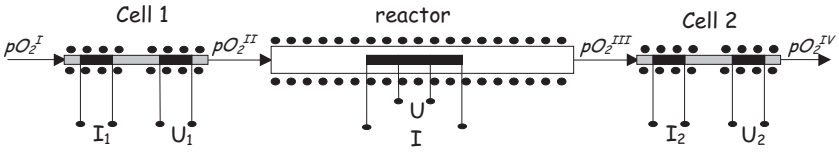

Fig. 2. Scheme of a solid electrolyte measurement device ZiroxySystem (Greifswald, Germany).

which is analogous to the OXYLYT system described elsewhere [9] (Fig. 2).

Direct current (dc) 4-point method was used for conductivity measurements. Both oxygen non-stoichiometry and electrical conductivity characteristics were measured simultaneously in air and in Ar/O_2 gas flow (pO_2 = 21,000, 23, 6, 2.4 and 0.6 Pa) in temperature range of 20–1000 °C. Porous as well as gas dense samples were used for the measurements. The conductivity of these samples was recalculated for non-porous samples using the following equation:

$$\sigma_d = \sigma_p \times \frac{1 + p/2}{(1-p)^{2/3}} \quad (1)$$

where p is the relative porosity, and σ_d and σ_p are the conductivities of dense and porous samples, respectively [10].

Phase stability of ceramic samples after treatment up to the maximum temperatures at every oxygen partial pressure was controlled after their cooling to room temperature by XRD.

2.4. Oxygen diffusion mobility and oxygen surface exchange

Chemical diffusion and oxygen surface exchange coefficients were determined by conductivity measurements of the gas dense sample obtained after every 50 °C temperature jumps from one equilibrium state to the other at every step. Temperature jumps up and jumps down were carried out at a rate of 40 °C min^{-1}. New equilibrium states were reached after 10–50 h exposure of the sample to new conditions depending on the temperature region and oxygen partial pressure e.g. progressively increasing exposure times were required for the sample to attain equilibrium with progressive increase in oxygen partial pressures. Relaxation parameters were determined in Ar/O_2 gas flow at oxygen partial pressures 21,000, 36, 23, 6, 2.4 and 0.6 Pa.

The analysis of the results of relaxation measurements was carried out using the solution of Fick's second law for a rectangular sample with the dimensions $2h \times 2w \times 2l$ by the following equation [11]:

$$\frac{\sigma_t - \sigma_0}{\sigma_\infty - \sigma_0} = 1 - \sum_{i=1}^{\infty}\sum_{m=1}^{\infty}\sum_{n=1}^{\infty} \frac{2L_1^2 \exp(-\beta_i^2 \tilde{D}_O t/h^2)}{\beta_i^2(\beta_i^2 + L_1^2 + L_1)} \times \frac{2L_2^2 \exp(-\gamma_m^2 \tilde{D}_O t/w^2)}{\gamma_m^2(\gamma_m^2 + L_2^2 + L_2)} \times \frac{2L_3^2 \exp(-\delta_n^2 \tilde{D}_O t/l^2)}{\delta_n^2(\delta_n^2 + L_3^2 + L_3)} \quad (2)$$

where σ_0, σ_∞, and σ_t denote the apparent conductivity at time $t = 0$ (initial), $t = \infty$ (after reaching a new equilibrium state) and time t (in the course of relaxation) respectively; $\tilde{D}_O$ is the chemical diffusion coefficient, t is the diffusion time. The dimensionless parameters L_1, L_2, and L_3 are defined using the linear oxygen exchange rate constant (α) and the chemical diffusion coefficient ($\tilde{D}_O$) as

$$L_1 = \frac{h\alpha}{\tilde{D}_O} \quad (2.1)$$

$$L_2 = \frac{w\alpha}{\tilde{D}_O} \quad (2.2)$$

$$L_3 = \frac{l\alpha}{\tilde{D}_O} \quad (2.3)$$

$$\beta_i \tan \beta_i = L_1 \quad (2.4)$$

$$\gamma_m \tan \gamma_m = L_2 \quad (2.5)$$

$$\delta_n \tan \delta_n = L_3 \quad (2.6)$$

which serve as a good measure of the significance of the surface reaction. Large and small L values correspond to diffusion-controlled and surface-reaction-controlled processes, respectively. β_i, γ_m, and δ_n are the nth roots of the Eqs. (2.4–2.6); $2h$, $2w$ and $2l$ are thickness, width and length respectively, of the sample with rectangular geometry.

This model of calculation is based on the following restrictions [11,12]:

(i) With small changes in oxygen non-stoichiometry (approximately 0.01 of the oxygen index) the diffusion parameters are assumed to be independent of the composition. In other words, the sample is assumed to maintain its composition within the whole volume before and after the temperature step.
(ii) The mobility of the charge carrier can be approximated as constant during the course of relaxation.
(iii) A linear relation should be assumed between the changes of the electrical conductivity and the concentration of the lattice oxygen or the oxygen vacancies.
(iv) The surface reaction kinetics is linear with respect to the oxygen concentration at the surface.
(v) The polycrystalline samples are assumed to be isotropic.
(vi) The value of the diffusion coefficient was related to the final temperature after each step.

The accuracy of the relaxation measurements is however limited by

(i) errors in the measurement of the geometrical dimensions of the sample.
(ii) different ceramic microstructures of samples as a result of ceramic preparation of powders, pressing and sintering conditions.
(iii) the experimental uncertainty of a "dead time" after a leap in temperature is captured by the sample.

3. Results and discussion

3.1. Structural and thermal characterisation

A portion of the $PrNi_{0.4}Fe_{0.6}O_{3-\delta}$ powder prepared at 1000 °C was heated at 1350 °C for 17 h and then cooled to room temperature before it was analysed further by synchrotron measurements. The resulting mass was crushed and ground to form a powder. It was black in colour and analysed by powder diffraction of synchrotron radiation to be single-phase orthorhombic perovskite with Pbnm space group (Fig. 3), where the degree of orthorhombic distortion is characterised by the tilting of the BO_6 octahedra. X-ray diffractograms recorded at 1000 °C and 1350 °C showed no difference in patterns confirming a pure single phase formation.

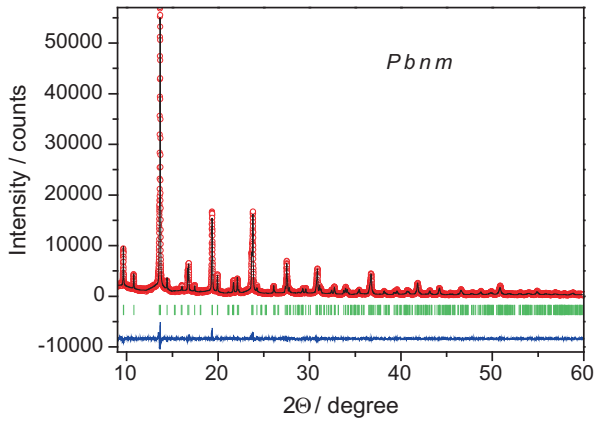

Fig. 3. Graphical results of Rietveld refinement for $PrNi_{0.4}Fe_{0.6}O_{3-\delta}$. Open circles (red) indicate experimental data, the line (black) through the open circles is the calculated profile and the lowermost plot (blue) is their difference. The ticks (green) in between the 2 profiles show the calculated positions of reflections. (For interpretation of the references to color in this figure legend, the reader is referred to the web version of this article.)

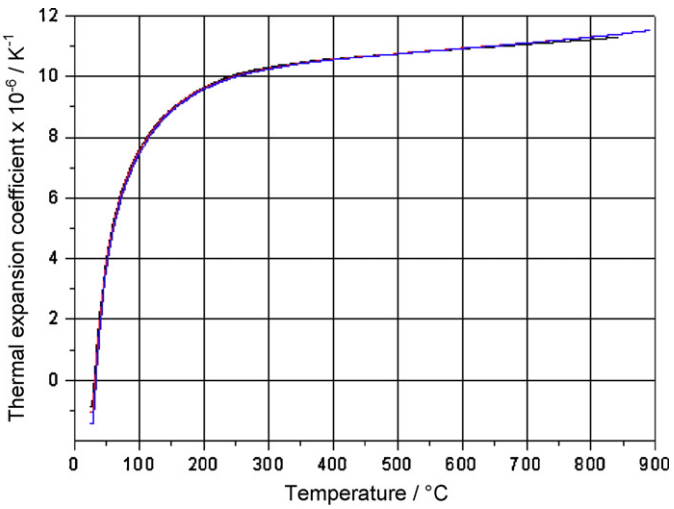

Fig. 5. Thermal expansion coefficients of the porous $PrNi_{0.4}Fe_{0.6}O_{3-\delta}$ ceramic samples measured in air at the rate of 10 °C min^{-1}. Heating curve (red) and cooling curve (blue). (For interpretation of the references to color in this figure legend, the reader is referred to the web version of this article.)

The temperature dependent diffraction data of $PrNi_{0.4}Fe_{0.6}O_{3-\delta}$showed linear changes in lattice parameters and cell volume and revealed no phase transitions in air conditions in the temperature range of 20–900 °C as shown in Fig. 4.

Expansion in *a* and *c* directions of the orthorhombic lattice is characterised by TEC of $13.7 \times 10^{-6}\,K^{-1}$ and in *b* direction by $6.7 \times 10^{-6}\,K^{-1}$. These are in good agreement and comparable with the TEC's found by dilatometric measurements in air over 100 °C (Fig. 5). As shown in Fig. 5, $PrNi_{0.4}Fe_{0.6}O_{3-\delta}$ has a TEC value of $10.5 \times 10^{-6}\,K^{-1}$ at 400 °C which gradually increases to about $11.4 \times 10^{-6}\,K^{-1}$ at 800 °C. These values are very near to those of the conventionally used electrolytes YSZ (TEC of $11 \times 10^{-6}\,K^{-1}$) and CeO_2 (TEC of $\sim 11.6 \times 10^{-6}\,K^{-1}$). Thus it would be interesting to study the combination of such a cathode with conventional electrolytes since the thermal stress at the interface and hence cracking and delamination of the fuel cell would be greatly reduced at operating temperatures.

Fig. 6 shows three different surface SEM images of the sample after high temperature investigations. The surface morphology is seen to be rough in Fig. 6(a). This could result in quicker oxygen exchange in this case. Closer examination shows no visible micro- or mesoporosity in the sintered samples. The ratio of the grain boundary section to the bulk diffusion section is very low and hence we believe that the diffusion process is controlled by the bulk diffusion of oxygen. This process is well explained by the model used in our work.

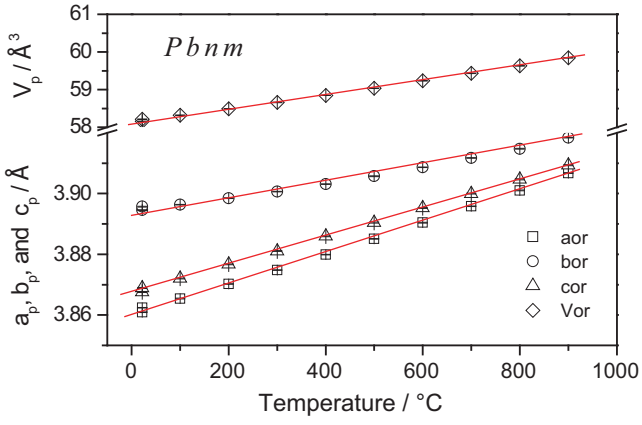

Fig. 4. Dependence of lattice parameters of the $PrNi_{0.4}Fe_{0.6}O_{3-\delta}$ powder on temperature determined in air.

3.2. Oxygen content and electrical conductivity

Electrical conductivity and oxygen exchange characteristics of the porous ceramic sample at pO_2 of 23 Pa during stepwise temperature jumps are presented in Fig. 7. Oxygen content values of the sample at room temperature before stepwise heating and after subsequent cooling processes coincide (plot 2) and this can be considered as an indication of phase stability of $PrNi_{0.4}Fe_{0.6}O_{3-\delta}$ at these conditions. Room temperature powder XRD patterns of the sample measured before and after this treatment proved the phase stability of the sample.

The time dependences of the parameters presented in Fig. 7 indicate fast equilibration of the $PrNi_{0.4}Fe_{0.6}O_{3-\delta}$ porous sample at pO_2 of 23 Pa after the mentioned temperature jumps. Plot 1 shows titration current in which deviation from the base level is a measure of amount of oxygen released (minimum) or absorbed (maximum) during the heating or cooling processes, respectively. Using this titration current, the actual oxygen content in the ceramics can be calculated accurately during the entire course of the experiment and is shown as Plot 2. Also, conductivity changes and temperature steps are clearly shown by Plots 3 and 4, respectively. Some characteristics observed during the course of this experiment can be summarized as follows:

(i) The sample is stable at pO_2 of 23 Pa up to a temperature of about 600 °C (Plots 1 and 2).
(ii) Between 600 C and 800 °C uptake of oxygen is small but measurable with corresponding increase in conductivity (Plot 3).
(iii) In the temperature range of 800–1000 °C loss of oxygen is higher than that between 600 °C and 800 °C. Correspondingly, the conductivity increases slightly at some intermediate temperature which then decreases to be stable at 1000 °C. This shows that conductivity depends not only on temperature but also on the oxygen content of the ceramics. During the cooling steps one observes absorption of a proportional amount of oxygen similar to that lost during the entire heating process.

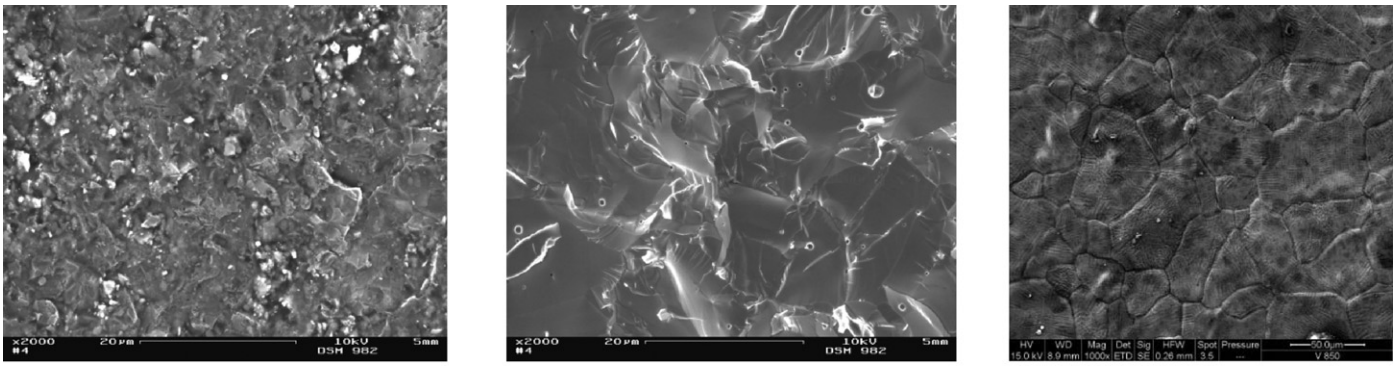

Fig. 6. SEM images of the already investigated sample: surface of entire sample (a), rough surface after breaking the sample in the middle into two halves (b), and polished surface of one of the broken halves of the sample (c).

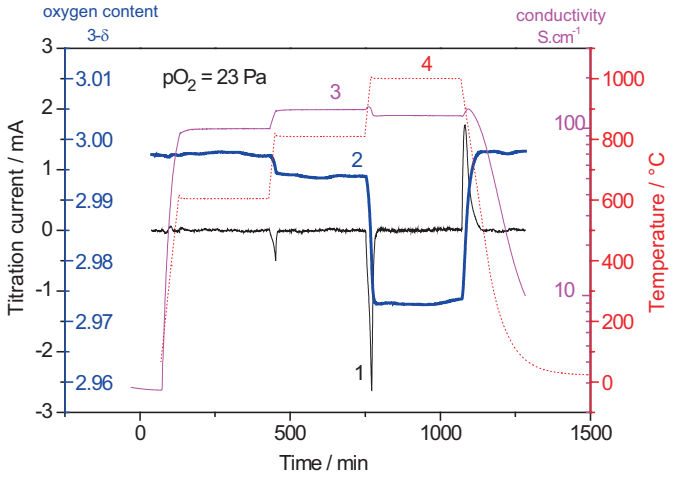

Fig. 7. Time dependences of titration current in coulometric cell 2 of ZiroxySystem device (plot 1), oxygen content (plot 2), conductivity (plot 3) and temperature (plot 4) of the $PrNi_{0.4}Fe_{0.6}O_{3-\delta}$ ceramic sample in Ar/O_2 gas flow at $pO_2 = 23$ Pa.

Conductivity of the $PrNi_{0.4}Fe_{0.6}O_{3-\delta}$ceramics was found to increase with increasing temperature over the range from room temperature to 1000 °C in air and at pO_2 of 6 Pa and as a small maximum at pO_2 of 23 Pa. This maximum in conductivity is caused by the changing oxygen content of the sample during the cooling process. In the cooling curves in Fig. 8, it can be observed that activation energy (E_a) increases from 0.1 eV in air (21,000 Pa of oxygen) to 0.12 eV at pO_2 of 23 Pa and finally to 0.14 eV at pO_2 of 6 Pa. This can be explained as to be due to the restriction of electron transfer through the –B–O–B–O– chains because of the higher concentration of oxygen vacancies created due to the increase in temperature and decrease of oxygen concentration in gas phase.

Also, conductivity was found to increase with increasing oxygen partial pressure and can be attributed to p-type conductivity. No linear dependencies in log(conductivity) vs. log(pO_2) coordinates were observed in the whole pO_2 range (6–21,000 Pa) at 400, 600, 800 and 1000 °C (Fig. 9). The parameter (k) in equation $\sigma = \sigma_0 \cdot (pO_2)^k$ has been varied between +1/30 and +1/4 depending on the temperature and oxygen partial pressure ranges as shown in Fig. 9. Low pO_2 range is characterised by higher k values. Since, no additional intermediary oxygen concentrations were studied between 23 and 21,000 Pa, an exact conductivity dependence in this pO_2 range is not available. It is possible that in oxygen rich atmospheres this compound is stable and its conductivity is independent of pO_2 particularly at low temperatures. The low oxygen partial pressure range is then characterised with the k parameter varied between +1/4 and +1/6.

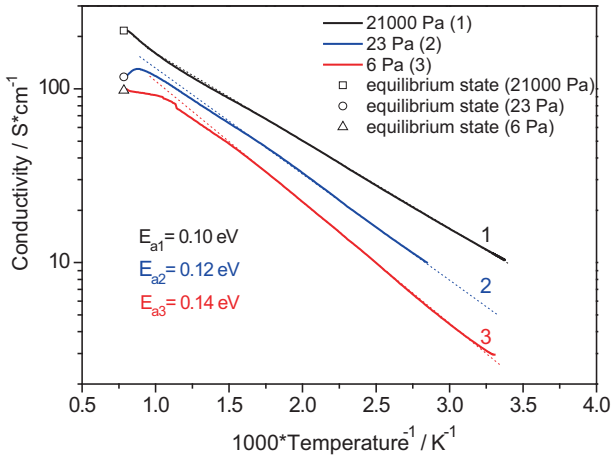

Fig. 8. Dependence of conductivity of the $PrNi_{0.4}Fe_{0.6}O_{3-\delta}$ ceramic sample at three different oxygen partial pressures on temperature during cooling process.

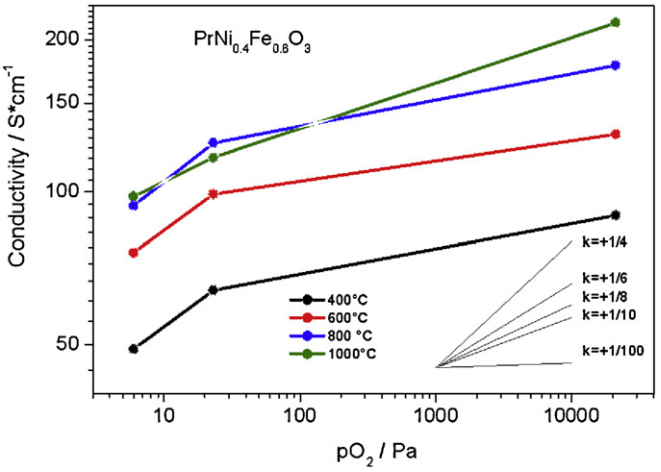

Fig. 9. pO_2 dependence of the electrical conductivity of the $PrNi_{0.4}Fe_{0.6}O_{3-\delta}$ ceramic sample.

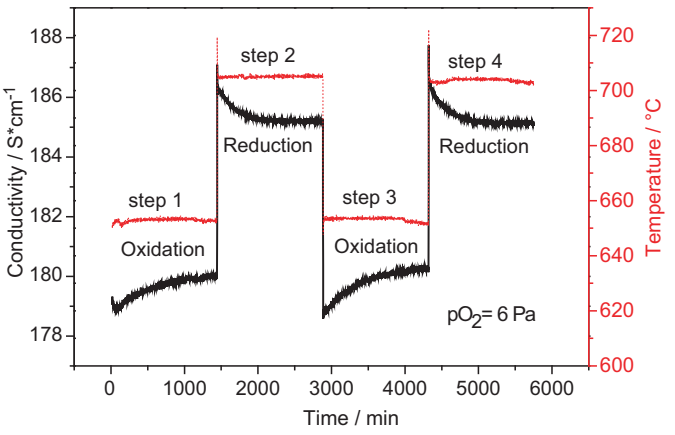

Fig. 10. A typical measurement of conductivity relaxation during stepwise change in temperature.

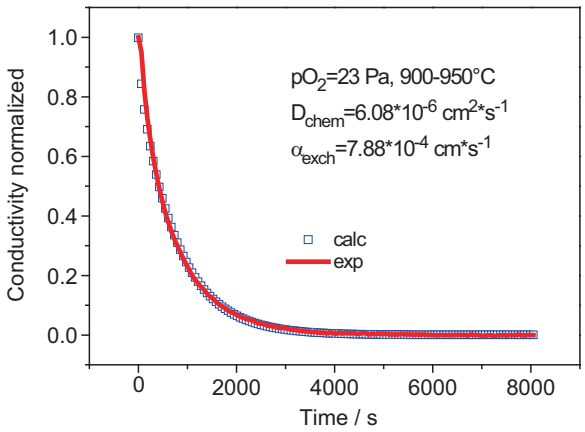

Fig. 11. A typical exponential decay curve of the relative conductivity with time during stepwise change in temperature at constant oxygen concentration in gas phase.

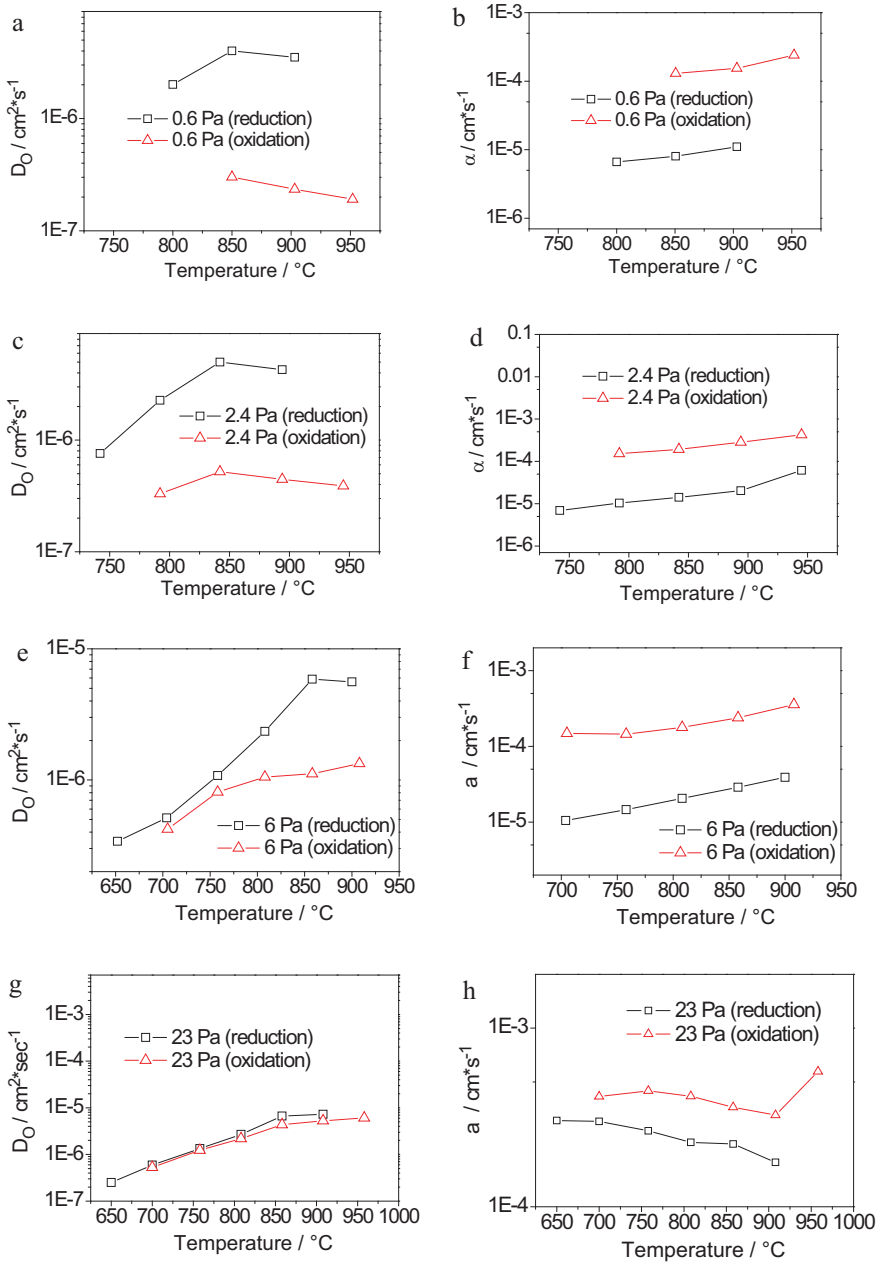

Fig. 12. Dependence of chemical diffusion ($\tilde{D}_O$) and oxygen surface exchange (α) coefficients (measured at different oxygen partial pressures) on temperature.

3.3. Chemical diffusion coefficient ($\tilde{D}_O$) and oxygen surface exchange rate (α)

Fig. 10 shows typical results of one of the relaxation experiments used in the calculation of oxygen diffusion and surface exchange characteristics on gas dense $PrNi_{0.4}Fe_{0.6}O_{3-\delta}$ceramic sample in Ar/O_2 gas flow at pO_2 of 6 Pa. It demonstrates the fact that such stepwise measurements can yield reproducible and reversible results when switching between two temperatures and the sample is allowed enough time to attain its new equilibrium state. For example, in Fig. 10, both reduction steps 2 and 4 show almost equal changes in conductivity and hence their diffusion characteristics were obtained and found to be comparable. However, since the initial equilibrium state was not reached, it is difficult to calculate the diffusion coefficient in oxidation step 1 and compare it with that calculated from step 3. Hence, diffusion data in all other temperature steps have been calculated and presented only for the third (oxidation) and fourth (reduction) steps.

Similar conductivity values obtained at 700 °C before and after treatment of the sample at 650 °C pointed to stability of the sample during this treatment and reversible change of its conductivity and hence its oxygen content. Analogous measurements were performed in air and in Ar/O_2 gas flow at pO_2 23, 2.4 and 0.6 Pa by temperature jumps $650 \rightarrow 705 \rightarrow 758 \rightarrow 808 \rightarrow 858 \rightarrow 908$ °C and then followed by cooling steps with the same temperature jumps in the opposite direction.

Fig. 11 illustrates good conformance of calculated and experimental $(\sigma_t - \sigma_0)/(\sigma_\infty - \sigma_0)$ values measured at pO_2 of 6 Pa after temperature jump of 900–950 °C for the proposed oxygen surface exchange constant (α) and the chemical diffusion coefficient ($\tilde{D}_O$). This shows that the conductivity relaxation kinetics has been well described by the model chosen in Section 2.4 which considers relaxation process control by both partial bulk oxygen diffusion and oxygen surface reaction. Due to the small ratio of grain boundary to volume sections of the sample (Fig. 6c) the ascertained diffusion coefficients can be attributed to volume chemical diffusion of oxygen.

The calculated chemical diffusion coefficients ($\tilde{D}_O$) and oxygen surface exchange rates (α) determined in Ar/O_2 gas flow at pO_2 0.6, 2.4, 6 and 23 Pa are presented in Figs. 12 and 13. The oxygen diffusion coefficients determined by stepwise heating of the sample (reduction) are higher in comparison with the coefficients determined by cooling of the samples (oxidation) as shown in Fig. 12a, c, e and g. This can be explained by lower concentration of oxygen vacancies which are dispersed in a statistically regular manner in the sample at lower temperatures. This actually means the sample at the beginning of the reduction processes was characterised with lower oxygen vacancy concentration as compared to when it underwent oxidation processes.

It is possible that oxygen vacancies form neutral defect clusters of the type $\langle B–V_O–B\rangle$, which as shown by van Roosmalen and Cordfunke [13] are not suitable for transport of oxygen ions, and thus reduce the concentration of "free" vacancies available for oxygen transport. The tendency to form ordered structures progressively grows with increasing defect concentration [14]. The concentration of oxygen vacancies is higher at lower pO_2 and hence formation of such clusters at lower pO_2 is more probable. The difference between diffusion coefficients determined during reduction and oxidation temperature jumps decreases with increasing pO_2 due to the lowering of oxygen vacancy concentration and the corresponding decrease in the difference in "free" vacancy and cluster concentration in the sample by reduction and oxidation processes. The increase in $\tilde{D}_O$ with oxygen partial pressure presented in Fig. 13a could be understood also by oxygen cluster formation. We do not discuss the nature of these clusters in this work. Reduction coefficients show a small maximum near 850 °C which can be explained also by the cluster formation theory.

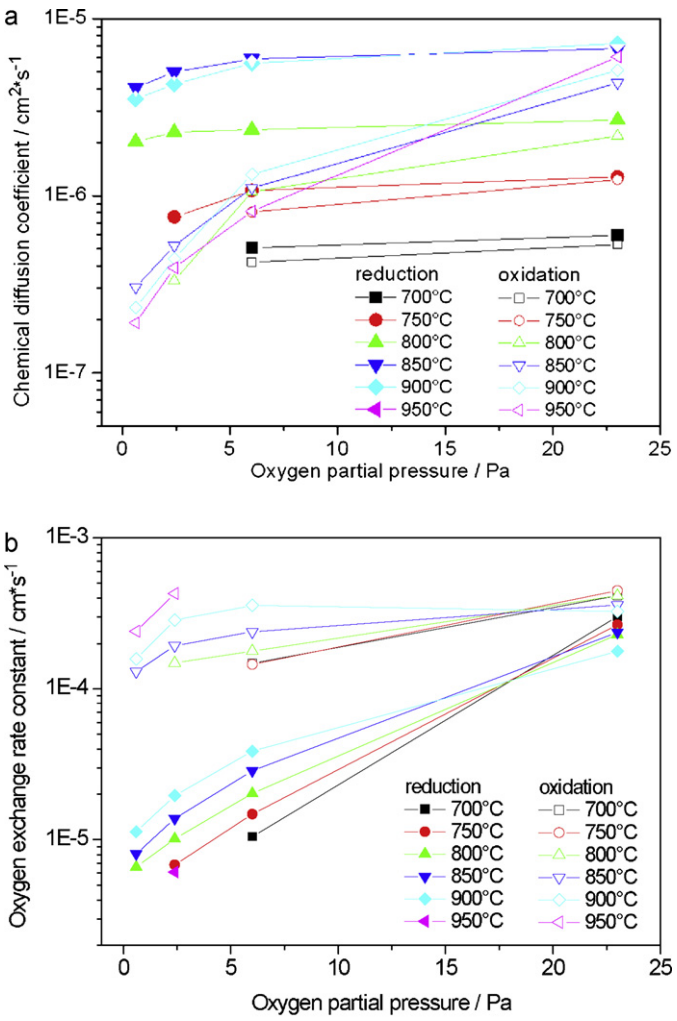

Fig. 13. Oxygen partial pressures dependence of chemical diffusion coefficients (a) and oxygen exchange rate constants (b) measured at different temperatures.

Despite numerous studies of oxygen exchange on the surface of mixed conducting oxides, the fundamental understanding of these reactions still remains very limited. Adler et al. [15] suggest that for electron-carrier-rich mixed conductors oxygen exchange is governed by chemisorption or dissociative adsorption on limited surface vacancy sites. This conclusion stands in contrast to conventional wisdom, which usually assumes that dissociation due to an activation barrier is the limiting process. The authors note that equilibrium exchange rates are inherently ambiguous probes of mechanism, often consistent with numerous possible mechanisms.

In contrast to chemical diffusion coefficients, the oxygen surface exchange coefficients of $PrNi_{0.4}Fe_{0.6}O_3$ (Fig. 12b, d, f, and h) for reduction processes are lower as compared with oxidation ones. Taking into consideration the conclusions [15] that oxygen exchange is determined by adsorption of oxygen on limited surface vacancy sites and accepting the fact that $PrFe_{1-x}Ni_xO_3$ is an electron-carrier-rich mixed conductor, the lower oxygen exchange coefficient for reduction processes could be explained by the lower concentration of oxygen vacancies in the initial sample independent of the above mentioned cluster formation.

Except for the highest pO_2 of 23 Pa, the α values increase with temperature at constant oxygen concentration (Fig. 12h).

4. Conclusions

$PrNi_{0.6}Fe_{0.4}O_{3-\delta}$ was found to be phase stable at $pO_2 > 1$ Pa up to 1000 °C. In the temperature range 400–1000 °C and pO_2 from 1 to 21,000 Pa it is a p-type semiconductor showing low conductivity versus pO_2 dependence. Oxygen non-stoichiometry reaches 0.06 of oxygen atomic index during heating in Ar flow at 1000 °C for 20 h. The thermal expansion coefficient of the investigated material varies from $10.5 \times 10^{-6}\,K^{-1}$ at 400 °C to about $11.4 \times 10^{-6}\,K^{-1}$ at 800 °C and hence makes it a favourable cathode material to be used in combination with the conventionally used YSZ and CeO_2 electrolytes.

Chemical diffusion coefficients vary between 1×10^{-5} and $2 \times 10^{-7}\,cm^2\,s^{-1}$ depending on oxygen partial pressure (0.6–23 Pa) and temperature jumps (750–950 °C). The calculated higher oxygen diffusion mobility for reduction processes in comparison with those for oxidation is explained by formation of neutral defect clusters of the type $\langle B–V_O–B\rangle$, which reduce the concentration of "free" oxygen vacancies available for oxygen transport. The oxygen diffusion is believed to be a bulk process and was supported and well explained by the proposed mathematical model.

Oxygen surface exchange coefficients of $PrNi_{0.4}Fe_{0.6}O_3$ for reduction processes are lower as compared with oxidation processes and are explained by the lower concentration of limited surface vacancy sites on the surface of the sample independent of formation of the $\langle B–V_O–B\rangle$-type clusters.

Acknowledgements

The authors gratefully acknowledge the financial support of the European Union and the Government of Saxony, Germany (SAB project 14252) and the DFG Graduiertenkolleg 1401 of the Dresden University of Technology.

References

[1] E.P. Murray, M.J. Sever, S.A. Barnett, Solid State Ionics 148 (2002) 27–34.
[2] S. Hashimoto, K. Kammer, F.W. Poulsen, M. Mogensen, J. Alloys Compd. 428 (2007) 256–261.
[3] R. Kumar, R. Choudhary, M. Ikram, D. Shukla, S. Mollah, P. Thakur, K. Chae, B. Angadi, W. Choi, J. Appl. Phys. 102 (2007) 073707.
[4] W.R. Cannon, M. Yoshimura, J. Mizusaki, T. Sasamoto, R.L. Pober, I. Hart, H.K. Bowen, J.F. Louis, Proc. 17th Symp. Eng. Aspects of MHD, Stanford University, March, 1978.
[5] J. Mizusaki, W.R. Cannon, H.K. Bowen, J. Am. Ceram. Soc. 63 (1980) 391–397.
[6] M. Knapp, C. Baehtz, H. Ehrenberg, H. Fuess, J. Synchrotron Rad. 11 (2004) 328–334.
[7] M. Knapp, V. Joco, C. Baehtz, H.-H. Brecht, A. Berghaeuser, H. Ehrenberg, H. von Seggern, H. Fuess, Nucl. Instrum. Methods A 521 (2004) 565–570.
[8] http://www-llb.cea.fr/fullweb/powder.htm.
[9] V. Vashook, L. Vasylechko, J. Zosel, W. Gruner, H. Ullmann, U. Guth, J. Solid State Chem. 177 (2004) 3784.
[10] R.E. Carter, W.L. Roth, General Electric Report 63-RL-3479 M, November 1963.
[11] I. Yasuda, M. Hishinuma, J. Solid State Chem. 123 (1996) 382–390.
[12] V. Vashook, M. Al Daroukh, H. Ullmann, Ionics 7 (2001) 1–8.
[13] J.A.M. van Roosmalen, E.P.H. Cordfunke, J. Solid State Chem. 93 (1991) 212–219.
[14] H.J.M. Bouwmeester, A.J. Burggraaf, in: P.J. Gellings, H.J.M. Bouwmeester (Eds.), CRC Handbook of Solid State Electrochemistry, CRC Press, Boca Raton, FL, 1997 (Chapter 14).
[15] S.B. Adler, X.Y. Chen, J.R. Wilson, J. Catal. 245 (2007) 91–109.